Tuning the magnetic properties of GaAs:Mn/MnAs hybrids via the MnAs cluster shape

H-A Krug von Nidda[1], T Kurz[1], A Loidl[1], Th Hartmann[2], P J Klar[2], W Heimbrodt[2], M Lampalzer[2], K Volz[2] and W Stolz[2]

[1] Experimental Physics V, Elektronic Correlations and Magnetism, Institute for Physics, Augsburg University, 86135 Augsburg, Germany
[2] Department of Physics and Material Sciences Center, Philipps University, Renthof 5, 35032 Marburg, Germany

E-mail: kvn@physik.uni-augsburg.de and peter.klar@physik.uni-marburg.de

Abstract

We report a systematic study of ferromagnetic resonance in granular GaAs:Mn/MnAs hybrids grown on GaAs(001) substrates by metal–organic vapour-phase epitaxy. The ferromagnetic resonance of the MnAs clusters can be resolved at all temperatures below T_c. An additional broad absorption is observed below 60 K and is ascribed to localized charge carriers of the GaAs:Mn matrix. The anisotropy of the MnAs ferromagnetic resonance field originates from the magneto-crystalline field and demagnetization effects of the ferromagnetic MnAs clusters embedded in the GaAs:Mn matrix. Its temperature dependence basically scales with magnetization. Comparison of the observed angular dependence of the resonance field with model calculations yields the preferential orientation and shape of the clusters formed in hybrid layers of different thickness (150–1000 nm) grown otherwise at the same growth conditions. The hexagonal axes of the MnAs clusters are oriented along the four cubic GaAs space diagonals. Thin layers contain lens-shaped MnAs clusters close to the surface, whereas thick layers also contain spherical clusters in the bulk of the layer. The magnetic properties of the hexagonal MnAs clusters can be tuned by a controlled variation of the cluster shape.

1. Introduction

Spin electronics and spin optoelectronics may be key technologies of the future, which combine the merits of current semiconductor-electronic and magneto-electronic devices. These technologies will provide new spin-dependent magneto-optical and magneto-electrical devices [1]. The current interest in spintronic devices has started a quest for new semiconductor-based magnetic materials such as ferromagnetic semiconductors [2] or

semiconductor–ferromagnet hybrid structures [3]. Possible candidates, which may serve as spin-aligner or spin-injector material and are compatible with III–V semiconductor technology, are the ferromagnetic phases of the (Ga, Mn)As system. The $Ga_{1-x}Mn_xAs$ alloy is p-type and exhibits ferromagnetism. Considerable progress has been made in the sample preparation of this alloy and Curie temperatures of about $T_C = 175$ K have been reported for GaAs delta-doped with Mn [4] as well as for epitaxial layers of the $Ga_{1-x}Mn_xAs$ alloy with x up to 9% [5]. Nevertheless, the spin-dephasing times for holes are much faster than for electrons and the observed Curie temperatures are still below room temperature. Therefore, the alloy is currently not suitable for room-temperature spin applications although recent theoretical and experimental studies suggest that room-temperature ferromagnetism is possible in high-quality metallic $Ga_{0.9}Mn_{0.1}As$ alloy samples [6]. Another interesting phase of this material system is formed by ferromagnetic MnAs clusters embedded in a paramagnetic GaAs:Mn host matrix. This hybrid system allows n-type doping of the matrix [7] and exhibits ferromagnetism above room temperature due to the MnAs clusters. Furthermore, considerable progress has been made in controlling the crystallographic properties of the MnAs clusters. This control comprises the crystal structure of the nanoclusters (i.e. cubic zinc blende structure or hexagonal NiAs structure) [8–10] as well as the orientation of the MnAs crystallographic axes with respect to the surrounding GaAs:Mn matrix [11].

Recently, such granular ferromagnetic hybrid systems have attracted much attention [9, 12–28]. The reasons are manifold. First, these hybrids exhibit large negative and positive magneto-resistance effects whose origin is still not entirely understood [19, 20, 23, 28]. Examples are current studies of the magneto-resistance behaviour of GaAs:Mn/MnAs [15, 19, 20, 28], of GaAs:Er/ErAs [21], of GaAs:Mn/MnSb [22] or of Ge:Mn/$Mn_{11}Ge_8$ and Ge:Mn/Mn_5Ge_3 [23, 26, 27]. Second, several studies of GaAs:Mn/MnAs hybrids and optical semiconductor-device structures containing this hybrid exhibit giant magneto-optical effects which should be applicable in optical insulator structures [13, 15, 29, 30]. Both the galvano-magnetic as well as the magneto-optical properties of such granular ferromagnetic hybrid systems will be strongly determined by the ferromagnetism of the clusters and their interaction with the electronic states of the host matrix. Therefore, it is of interest to investigate the magnetic behaviour of the clusters themselves.

At present there are only very few detailed studies of the ferromagnetism of such MnAs clusters [9, 31]. Recently, there were a few reports on ferromagnetic resonance (FMR) studies investigating spin waves in ferromagnetic $Ga_{1-x}Mn_xAs$ layers and on deducing the magnetic anisotropy of the layers [32–34]. We have previously shown that FMR is a useful tool for determining the orientation of hexagonal MnAs clusters embedded in the GaAs:Mn host matrix [31]. Due to the pronounced magneto-crystalline anisotropy of MnAs, the resonance field of the FMR signal strongly depends on the orientation of the external magnetic field with respect to a MnAs cluster. From the observed angular dependence the hexagonal MnAs [0001] axis was found to be aligned parallel to the cubic GaAs [111] axis. In (Ga, Mn)As grown on GaAs (111)A substrates the hexagonal axis of the magnetically dominant MnAs clusters is aligned perpendicular to the plane of the substrate. On GaAs(001) substrates all four possible orientations of the MnAs clusters in the GaAs:Mn matrix are detected.

Here, we will focus in particular on a set of granular GaAs:Mn/MnAs hybrid samples grown by metal–organic vapour-phase epitaxy (MOVPE) for which we have demonstrated that the transport properties are dominated by cluster effects [28]. We present a systematic FMR investigation of GaAs:Mn/MnAs hybrids of different layer thickness 150 nm $\leqslant d \leqslant$ 1000 nm grown on GaAs(001) substrate. We will show that the FMR contains important information not only on the orientation but also on the shape of the MnAs clusters formed in samples of different layer thickness. We will discuss the relation between the observed magnetic anisotropy and the

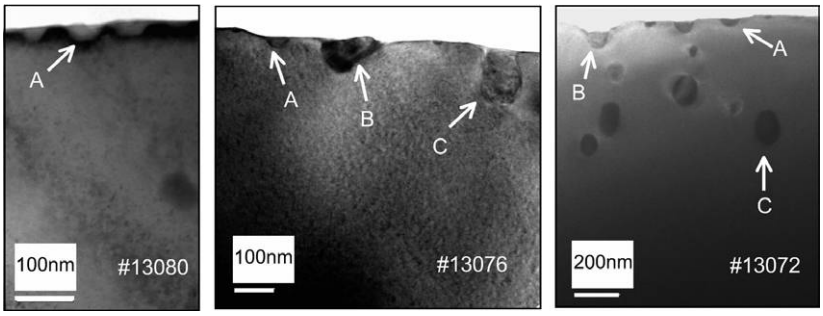

Figure 1. Transmission-electron microscope images of GaAs:Mn/MnAs layers of different thickness (left: 150 nm, centre: 500 nm, right: 1000 nm). Three types of cluster shape labelled A, B, C can be distinguished.

transport properties. Comparative transmission-electron microscope (TEM) measurements will corroborate these results.

2. Sample preparation and characterization

Hybrid structures consisting of a paramagnetic GaAs:Mn matrix and ferromagnetic MnAs clusters were grown by MOVPE as described in [35]. The layers were grown on GaAs(001) substrates at a growth rate of 0.5 μm h^{-1}, a V/III-ratio of 5, and a nominal Mn/Ga ratio of 24% in the gas phase. For all samples under investigation the growth temperature was kept at 500 °C. A series of four samples of different layer thicknesses (150, 300, 500 and 1000 nm), but otherwise unaltered growth conditions was grown. Under these growth conditions, MnAs clusters are formed within a GaAs:Mn matrix with Mn-doping levels of about 10^{19} cm^{-3}.

To characterize the MnAs clusters formed during the MOVPE growth process further, detailed TEM investigations were performed with a JEOL 3010 microscope. Three types of MnAs cluster were found in the samples under study. Figure 1 exemplarily shows TEM images of the samples #13080, #13076 and #13072 with layer thicknesses of 150, 500 and 1000 nm, respectively. In the thin layer of 150 nm thickness (left image of figure 1), only one type of cluster (referred to as type A) is detected. These clusters possess a lens-like shape and are all situated close to the sample surface. A closer investigation yields average dimensions of $d_\parallel = 13$ nm and $d_\perp = 35$ nm parallel and perpendicular to the surface normal, respectively. The layer of 500 nm thickness (centre image of figure 1) contains, in addition to type A clusters, two other cluster types. These are a type B of lens-shaped clusters with a bigger $d_\parallel/d_\perp$ ratio than type A (i.e. closer to 1 but still smaller) and a type C with approximately spherical shape (i.e. $d_\parallel/d_\perp \approx 1$). All three types of cluster are situated close to the surface for the 500 nm layer. However, the clusters of type C are beginning to taper towards the surface, i.e. show a tendency to be overgrown. This is further confirmed by the TEM image of the 1000 nm layer (right image of figure 1). For this sample, clusters of type C can be found embedded in the bulk of the layer whereas clusters of the other two types remain mainly located close to the surface.

Table 1 summarizes the types of cluster found in the four different layers. The dominant type for each layer is indicated by a bold letter. It appears that with increasing layer thickness in the MOVPE growth the shape of the dominant clusters changes from lens-shaped clusters of type A to spherical clusters of type C. Type C appears to be the final stage of cluster formation. Typical cluster densities are about 140 clusters per μm^2, almost independent of the thickness of the layer [28, 36]. Details of the actual formation process of the clusters and the overgrowth

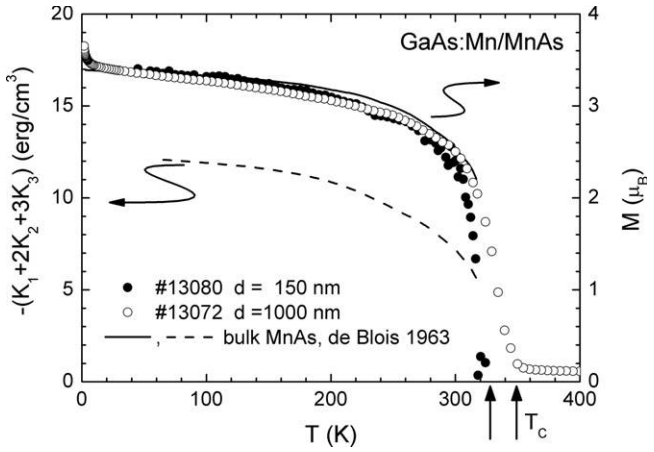

Figure 2. Right ordinate: temperature dependence of the magnetization for GaAs:Mn/MnAs layers #13080 ($d = 150$ nm) and #13072 ($d = 1000$ nm) (measured at 1000 Oe) normalized to data of MnAs single crystals taken from [38]. Left ordinate: corresponding magneto-crystalline anisotropy of MnAs single crystals also taken from [38].

Table 1. Characteristic parameters of the studied GaAs:Mn/MnAs layers grown on GaAs(001) substrates. The definition of the cluster types A, B and C is given in the text. The bold lettering indicates the dominant cluster type in each layer.

Sample no	Cluster types	Thickness (nm)
#13072	A, B, **C**	1000
#13076	A, B, **C**	500
#13077	A, **B**	300
#13080	**A**	150

process are described elsewhere [35, 37]. In brief, layers of MnAs clusters (type A) are formed at the surface, when the Mn concentration, which results from surface segregation, exceeds a critical value. The MnAs clusters continue to grow by a process where Ga is transported via diffusion to the bottom of the cluster, where GaAs:Mn with cubic zinc blende structure is formed, while MnAs is dissolved there and Mn diffuses to the top of the cluster, where MnAs is formed again. Thus, the cluster tends to remain located at the surface. During the growth process a certain amount of Ga is incorporated into the MnAs cluster. This growth continues until the cluster has reached a critical (final) size. Then the shape of the MnAs cluster changes and the cluster becomes fully embedded in the matrix (type C). It is not quite clear whether the shape transformation of the clusters from type A to type C is continuous or sudden shape changes occur during the growth process as only three types of cluster are detectable by TEM even for the thickest layer. The existence of a discrete number of cluster shapes is further corroborated by the FMR studies discussed below.

The temperature-dependent magnetization of the GaAs:Mn/MnAs hybrid samples follows the behaviour observed in pure MnAs [38] as shown exemplarily for the 150 nm layer #13080 and the 1000 nm layer #13072 in figure 2. All data have been normalized to the bulk magnetization of 3.4 μ_B at low temperatures. The best agreement is found for the thin layer. With increasing layer thickness deviations and a slight enhancement of the Curie temperature up to about 340 K with respect to $T_C = 318$ K of bulk MnAs [39] show up. This may originate from different sources, e.g. strain or the single-domain character of the clusters, or

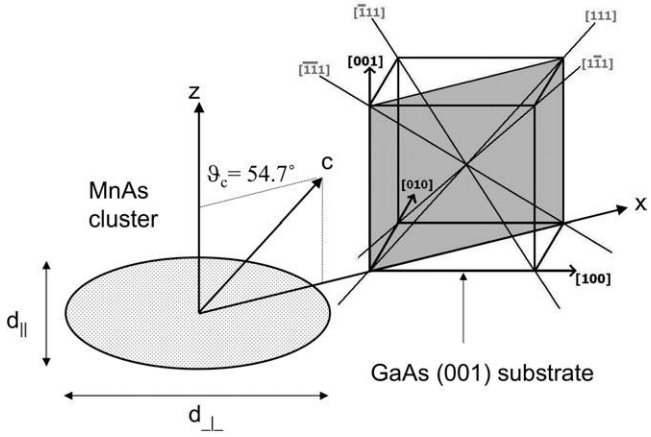

Figure 3. Geometry for the angular dependence measurements. The MnAs cluster is modelled as rotational ellipsoid with its symmetry axis parallel to the normal z of the GaAs(001) layer. The hexagonal MnAs [0001] c-axis is aligned along the GaAs [111] direction. The shadowed plane assigns the GaAs(110) plane of rotation.

the incorporation of a small fraction of Ga atoms into the clusters. As we will see, the shape of the clusters, which changes with the thickness of the layers, plays an important role for the effective anisotropy of the magnetization.

3. Model calculations

Before we present the experimental results in detail, we briefly introduce the theory of ferromagnetic resonance [40] required to model the expected anisotropy of the resonance field. We consider a ferromagnetic sample of magnetization $\mathbf{M}$ within an external static magnetic field $\mathbf{H}_{\text{ext}}$. The effective magnetic field $\mathbf{H}_{\text{eff}}$ acting on $\mathbf{M}$ includes the magneto-crystalline anisotropy field $\mathbf{H}_{\text{an}}$ determined by the lattice symmetry and the demagnetization field $\mathbf{H}_{\text{dem}}$ due to the shape of the ferromagnetic sample:

$$\mathbf{H}_{\text{eff}} = \mathbf{H}_{\text{ext}} + \mathbf{H}_{\text{an}} + \mathbf{H}_{\text{dem}}. \tag{1}$$

Without damping, the magnetization $\mathbf{M}$ precesses around the direction of $\mathbf{H}_{\text{eff}}$ with the Larmor frequency $\omega = \gamma H_{\text{eff}}$. Here $\gamma = g\mu_{\text{B}}/\hbar$ denotes the gyromagnetic ratio with the g value, Bohr magneton μ_{B}, and Planck constant $\hbar$. This uniform precession can be driven on resonance by a transverse magnetic microwave field $\mathbf{h}\cos(\omega t) \perp \mathbf{H}_{\text{ext}}$.

In general the directions of the three contributions to the effective magnetic field are not parallel to each other. Therefore it is useful to describe the resonance condition in terms of the energy density U as (Smit–Suhl formula) [40]

$$\left(\frac{\omega}{\gamma}\right)^2 = \frac{1}{M^2 \sin^2(\theta)}\left[\frac{\partial^2 U}{\partial\theta^2}\frac{\partial^2 U}{\partial\varphi^2} - \left(\frac{\partial^2 U}{\partial\theta\partial\varphi}\right)^2\right] \tag{2}$$

with the polar angle θ and the azimuth angle φ of the magnetization vector with respect to the chosen coordinate frame. The full geometry of the problem is illustrated in figure 3. The four possible orientations of the hexagonal c-axis of the MnAs cluster are given by the [111] space diagonals in the cubic GaAs:Mn matrix. They are characterized by the polar coordinates $\theta_c = 54.7°$ and $\varphi_c = 0°$, 90°, 180°, and 270°. Here the x-axis, which defines the zero point for φ, is chosen along the [110] direction, along which the film is usually cleaved. The

shadowed area indicates the (110) plane in which the external magnetic field is rotated during a measurement described by spherical coordinates $0 \leqslant \theta_H \leqslant 180°$ and $\varphi_H = 0$ or 180°. The other two rotation axes used in our experiments are the [110] axis ($0 \leqslant \theta_H \leqslant 180°$ and $\varphi_H = 90°$ or 270°) and the [001] axis ($0 \leqslant \varphi_H \leqslant 360°$ and $\theta_H = 90°$) forming an orthogonal system with the [110] axis.

The right-hand side of equation (2) resembles the square of the effective field $\mathbf{H}_{\text{eff}} = -\nabla_M U(\theta, \varphi)$. The energy density is given by the sum of Zeeman $U_{\text{Zee}} = -\mathbf{M} \cdot \mathbf{H}_{\text{ext}}$, anisotropy U_{an} and demagnetization $U_{\text{dem}} = \mathbf{M}(\mathbf{NM})/2$ energy with the demagnetization tensor $\mathbf{N}$. The resonance condition equation (2) has to be simultaneously fulfilled with the equilibrium condition for the magnetization at (θ_0, φ_0), where the energy density has to attain a minimum, i.e. the first derivatives of U with respect to θ or φ have to vanish and the second derivatives have to be larger than zero.

To evaluate equation (2) the magnetization $\mathbf{M}$ is written in polar coordinates as $M_x = M \sin\theta \cos\varphi$, $M_y = M \sin\theta \sin\varphi$, and $M_z = M \cos\theta$. The magnetic field $\mathbf{H}_{\text{ext}}$ and the c-axis direction $\mathbf{c}$ of the cluster are described analogously with the polar coordinates (H, θ_H, φ_H) and (c, θ_c, φ_c), respectively. Then the Zeeman energy reads

$$U_{\text{Zee}} = -M H_{\text{ext}}[\cos(\varphi - \varphi_H) \sin\theta \sin\theta_H + \cos\theta \cos\theta_H]. \tag{3}$$

The uniaxial magneto-crystalline anisotropy is expressed by

$$U_{\text{an}} = K_{\text{u}} \left\{1 - [\cos(\varphi - \varphi_c) \sin\theta \sin\theta_c + \cos\theta \cos\theta_c]^2\right\} \tag{4}$$

where we assume that the magneto-crystalline anisotropy energy can be confined to the dominant uniaxial contribution $K_{\text{u}} = K_1$ with respect to the crystallographic c-axis. This is justified by the single-crystal investigations of de Blois and Rodbell [38] who found that at 308 K the absolute value of the uniaxial contribution $K_1 = -5.75 \times 10^6$ ergs cm^{-3} is about four times larger than the higher-order terms $K_2 = +1.5 \times 10^6$ ergs cm^{-3} and $K_3 = -1.15 \times 10^6$ ergs cm^{-3}. Additionally, they determined the temperature dependence of the sum of $K_1 + 2K_2 + 3K_3$, which we show in figure 2 together with the magnetization data. Assuming that $2K_2$ and $3K_3$ approximately cancel each other also for lower temperatures, this yields a good estimate of the temperature dependence of K_1. The corresponding anisotropy field $H_{\text{A}} = K_1(T)/M(T)$ is approximately temperature independent with a value of about $H_{\text{A}} = 16$ kOe.

The different shapes of the clusters found by TEM can be approximated by rotational ellipsoids. The rotation-symmetry axis of the lens-shaped clusters (type A and B) near the film surface is oriented along the normal vector of the GaAs(001)-plane, which we choose as the z-axis of our coordinate system. Hence, the demagnetization tensor is diagonal with the components $N_z \equiv N_\parallel \propto 1/d_\parallel$ and $N_x = N_y \equiv N_\perp \propto 1/d_\perp$, which are determined by the inverse diameter of the cluster parallel ($d_\parallel$) and perpendicular ($d_\perp$) to its rotational axis and have to fulfil the normalization condition $N_x + N_y + N_z = 4\pi$. If the Cartesian coordinates coincide with the principal axes of the ferromagnetic ellipsoid, the shape anisotropy is written as

$$U_{\text{dem}} = \tfrac{1}{2} M^2 (N_x \sin^2\theta \cos^2\varphi + N_y \sin^2\theta \sin^2\varphi + N_z \cos^2\theta). \tag{5}$$

From these expressions (3)–(5) the first and second derivatives with respect to θ and φ are calculated analytically and inserted into equation (2) and into the minimization conditions for the free energy density U. For given values of M, K_{u}, N_x, N_y, N_z, θ_H, φ_H and ω the resonance field H_{res} is determined from the simultaneous numerical solution of the resonance condition and the minimization of U. The full angular dependence of the resonance field is obtained by performing this procedure for all angles θ_H, φ_H of interest.

4. Experimental results and discussion

The ferromagnetic resonance (FMR) measurements were performed with a Bruker ELEXSYS E500 CW-spectrometer in a rectangular H_{102} cavity at X-band frequency ($\nu \approx 9.35$ GHz). The temperature is varied by a helium continuous gas-flow cryostat (Oxford Instruments) working in the temperature range 4.2 K $\leqslant T \leqslant$ 300 K. The FMR spectra record the power P_{abs} absorbed by the sample from the transverse magnetic microwave field as a function of the static magnetic field H. The signal-to-noise ratio of the spectra is improved by detecting the derivative $\mathrm{d}P_{\mathrm{abs}}/\mathrm{d}H$ using a lock-in technique with 100 kHz field modulation. The GaAs films were glued on a suprasil-quartz rod, which allowed the rotation of the sample around defined crystallographic axes.

Figure 4 illustrates the FMR spectra and their anisotropy for the three characteristic sample orientations. As one can see in the inset, the spectra consist of at least two resonance lines with their resonance fields strongly dependent on the direction of the applied magnetic field. The solid line represents a fit by the field derivative of two Lorentzian curves on a linear background which accounts for microphone effects due to the field modulation technique. The main pictures give an overview of the angular dependence of the spectra. They represent a two-dimensional map of the dependence of the FMR signal on the magnetic field strength and orientation. The grey scale illustrates the signal amplitude as indicated by the spectrum in the inset.

The rotation within the (110) plane shows two identical curves ('one feature') with a periodicity of 180° each. They cross each other at 0° and 90°, giving rise to a mirror symmetry with respect to the GaAs [001] and [110] axes. Their minimum resonance field is located at approximately 3 kOe; the maximum field is beyond the limit of the experimental setup. The polar angles of these resonance maxima are near the GaAs [111] and [111] directions indicating the hard magnetic axes of MnAs clusters grown with their hexagonal c-axis along these two orientations. In the (110) plane, two more curves with the same symmetry become observable at lower resonance field (2 kOe in the minimum). Finally, in the (001) plane, basically no signal is noticeable except for those directions where the azimuthal angle hits the GaAs [110] and [110] axes. Due to higher amplification compared to the other two frames, angle-independent absorption lines show up at resonance fields of about 1.7 and 3.4 kOe. They originate from the background of cavity and substrate.

For further discussion, the resonance positions have been determined for all layer thicknesses and sample orientations. Most information can be obtained from the anisotropy within the (110) plane which is shown in figure 5(a). The thinnest layer exhibits only one resonance feature, the minimum of which is located at about 3.5 kOe. With increasing thickness (300 nm), this feature is found at slightly lower resonance field (3 kOe) and a second one appears at 1.9 kOe. The 500 and 1000 nm layers show a total of four features, with their minimum fields between 0.9 and 3.5 kOe.

To describe the resonance features, simulations have been carried out which are based on the model developed above. The magnetization and anisotropy constant are taken from [38]. The remaining fit parameters are the cluster shape, given by the ratio between height and width, and the crystallographic orientation of the hard axis of the MnAs cluster in the GaAs matrix. The latter is expected to be 54.74° due to the substrate orientation. This value has been used for the simulations in figure 5(a). It turned out that it is possible to describe all observed resonance features only by variation of the cluster geometry. The thin layer shows flat ('pancake') clusters with an N_z:N_x ratio of 0.25. For the 300 nm layer, two cluster types are necessary to describe the data: one with an N_z:N_x of 0.35 and another with 0.55. In the layers of 500 nm and above, nearly spherical (N_z:$N_x = 0.8$) clusters can be found in addition to the pancake-like ones. The determined N_z:N_x ratios between 0.25 and 0.8 are in good agreement with the TEM

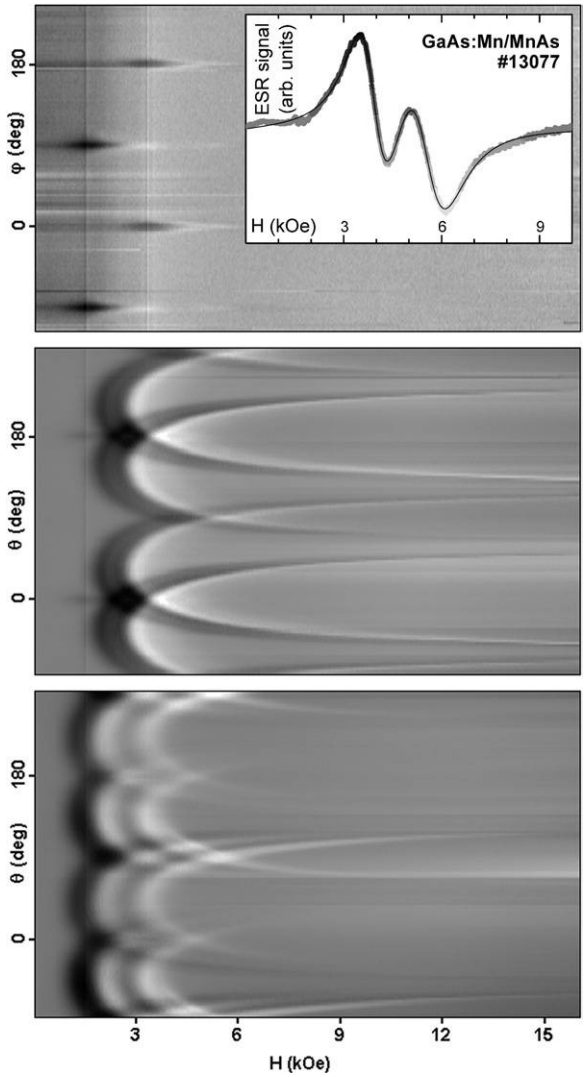

Figure 4. Angular dependence of the ferromagnetic resonance spectra in sample #13077 (d = 300 nm, T = 150 K) with the rotation axis parallel to GaAs [001] (magnetic field always within the layer), [110] and [110] (substrate orientations) directions (upper, middle and lower frame, respectively). Inset: typical spectrum at $\theta = 30°$ for rotation around the [110] axis (cf middle frame). The grey scale indicates the signal amplitude.

pictures. The small, intermediate and large ratios correspond to the clusters of type A, B and C, respectively.

The important result of this evaluation is the fact that only the shape of the clusters determines the changes in the magnetic properties of the hybrid system. The magnetization and its anisotropy are found to have the same values as bulk MnAs and therefore are independent of the cluster shape and size. Comparing the shift of the resonance maxima with increasing N_z:N_x, one nicely recognizes the competition between the magneto-crystalline anisotropy and the shape anisotropy. The magneto-crystalline anisotropy is the dominant contribution with the maximum of $H_{\max} = 35.0$ kOe at $\theta = 54.74°$ and analogous orientations. The

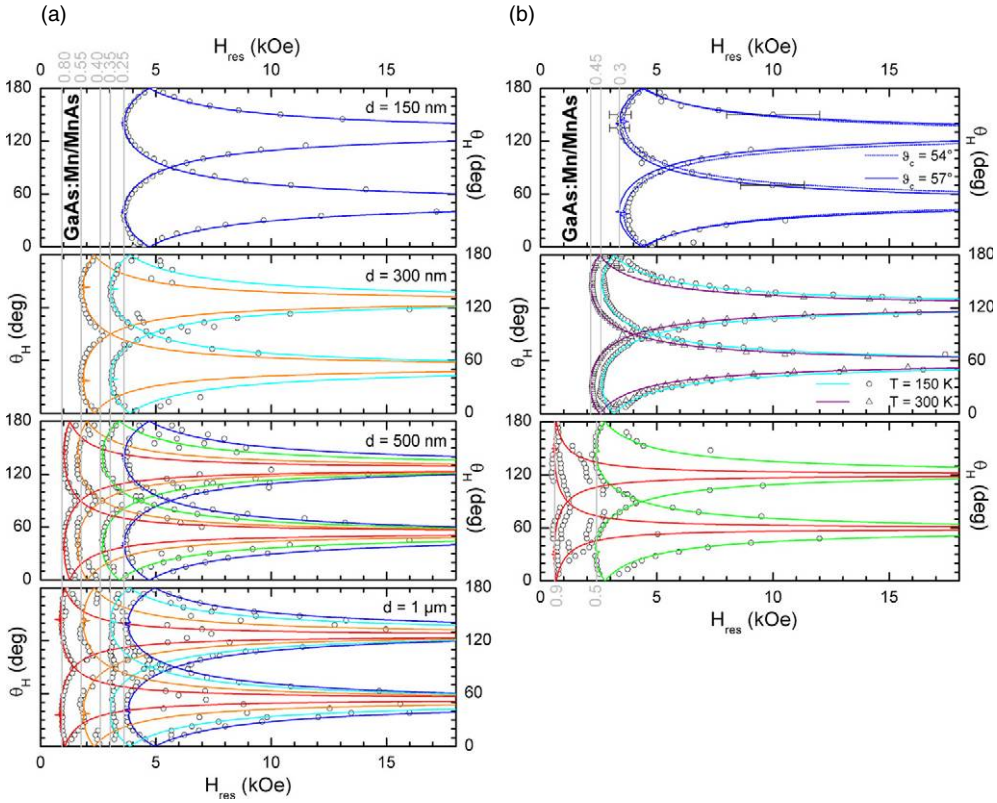

Figure 5. (a) Left side: angular dependence of the ferromagnetic resonance fields for all layer thicknesses d under consideration at $T = 150$ K with the rotation axis parallel to the GaAs [110] direction. The solid lines represent simulations for the N_x/N_z ratios given at the top for the respective resonance minima marked by straight dotted lines. (b) Right side: angular dependence of the ferromagnetic resonance fields for different layer thicknesses d (150, 300 and 1000 nm) at $T = 150$ K with the rotation axis parallel to the GaAs [110] direction. The solid lines represent simulations for the N_x/N_z ratios given at the top for the respective resonance minima marked by straight dotted lines. The horizontal bars in the upper frame indicate the linewidth at the respective resonance fields. The triangles in the middle frame mark the resonance positions at $T = 300$ K.

(This figure is in colour only in the electronic version)

shape anisotropy vanishes for spherical clusters, but it becomes evident for the pancake-shaped clusters with the preferred direction $\theta = 0°$ and therefore shifts the maximum down to $\theta = 50°$ ($H_{\max} = 35.5$ kOe). At the same time the minimum resonance field is evidently shifted to higher magnetic fields due to the competition of both anisotropy contributions as well.

Additional information and support of the above evaluation is obtained from the discussion of the FMR in the (110) plane (depicted in figure 5(b)). The thin layer again shows only one resonance feature with a minimum of around 3.5 kOe which now belongs to the other two possible MnAs cluster orientations in the GaAs matrix (i.e. [111] and [111]). However, a slight asymmetry is noticeable between the two curves. Furthermore, it turned out that a description with the MnAs hard axis exactly aligned along the GaAs [111] direction $\theta_c = 54.74°$ was not possible (dotted line). With a slightly increased angle ($\theta_c = 57°$; solid line), the description becomes better on one side of the curves, but worse on the other side. This means that we have a finite distribution of growth angles in this sample. With increasing layer thickness, the angle

stabilizes at $\theta_c = 60°$, which gives a satisfactory description of all resonance features in both the 300 and 1000 nm layer. It seems that the MnAs cluster growth with the c-axis along the GaAs [111] and [111] direction is preferred in comparison with the other two crystallographic directions. This is corroborated by the fact that in the thin layers (150 and 300 nm) the resonance fields observed in the (110) plane yield a larger N_z:N_x than those in the (110) plane of the same sample, i.e. the clusters of the former orientation are thicker and start to grow earlier during the MOVPE growth than those of the latter orientation.

Returning to figure 4 the azimuthal angular dependence shown in the upper frame proofs that there exist no preferred growth orientations for the MnAs clusters other than the GaAs space diagonals. Only when we meet the projection of these space diagonals onto the (001) plane, do distinct signals appear which from their resonance fields can be unambiguously ascribed to the corresponding MnAs clusters. For the other angles the FMR signal is strongly broadened and smeared out, thus revealing a finite distribution of the cluster axes and shapes. Nevertheless, the discrete number of FMR features observed in all layers proves that there is not a continuous distribution but some kind of quantization of the MnAs cluster shape, i.e. only a few preferred diameter ratios between thin pancakes at the surface and overgrown spheres in deeper regions exist.

The sharpness of the quantization of cluster shapes can be roughly estimated from the linewidths. As exemplarily indicated in the upper right-hand frame of figure 5, the linewidth of the signals increases from a few hundred Oe at low resonance fields (below 5 kOe) to some kOe at high fields (10–16 kOe). With increasing linewidth deviations from the Lorentzian line shape show up. This again suggests that the line broadening is dominated rather by 'macroscopic' cluster properties (orientation and shape) than by intrinsic relaxation. The width of the shape distribution can quantitatively be estimated by performing simulations with slightly varied N_z:N_x. Taking into account all N_z:N_x which yield resonance fields within the linewidth of a given angle-dependent resonance feature, one finds that the width-to-height ratio of the clusters varies by less than ± 0.1.

Now we turn to the temperature dependence of the FMR in the GaAs:Mn/MnAs layers. As already indicated in the middle frame of figure 5(b), the changes of the resonance-field anisotropy with temperature can be reasonably described by taking into account the temperature dependence of the magnetization. All other parameters are kept constant in the description of the angular dependence at 300 K as compared to that at 150 K. The full temperature dependence of the ferromagnetic resonance spectra is depicted in the left frame of figure 6 for the thin layer with $d = 150$ nm. At first one can see that the ferromagnetic resonance positions practically do not change below 150 K, corroborating the persistence of a nearly constant anisotropy down to the lowest temperatures. Besides, one observes that below about 60 K a broad absorption appears which extends as a dark shadow over the full accessible field range and increases with decreasing temperature. The anisotropy of this broad absorption is illustrated in the right frame at a temperature of $T = 4$ K. It is symmetric with respect to the normal of the layer and is shifted to high fields above the accessible range of the magnet for the magnetic field applied within the layer plane. At the same time the well known anisotropy of the thin lens-shaped MnAs clusters is visible. Again, the angle-independent absorption lines observed at resonance fields of about 1.7 and 3.4 kOe originate from the background of cavity and substrate. With increasing layer thickness the broad absorption signal quickly weakens. Already in the $d = 300$ nm layer one observes only a slight change of the background between 40 and 60 K.

At first glance one might assume that the broad absorption is due to an FMR signal of the GsAs:Mn matrix itself, but this can be ruled out as the Mn concentration in the matrix is smaller than 0.5%, i.e. the matrix remains paramagnetic down to the lowest temperatures accessible in our experiment. Furthermore, we found that the paramagnetic resonance signal of

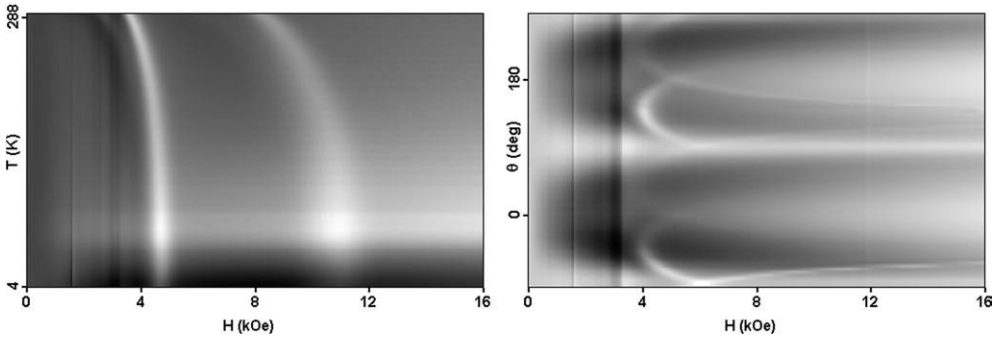

Figure 6. Left frame: temperature dependence of the ferromagnetic resonance spectra in sample #13080 ($d = 150$ nm, $\theta = 66°$). Right frame: corresponding angular dependence with the rotation axis parallel to the GaAs [110] direction at $T = 4$ K. The grey scale indicates the signal amplitude, as in figure 4.

Mn is too weak for detection in purely paramagnetic p-type GaAs:Mn layers of comparable thickness (without MnAs clusters). To understand this broad resonance absorption at low temperatures it is helpful to refer to the transport properties reported earlier [28]. There are two competing mechanisms which govern the magneto-resistance leading to a change from a positive magneto-resistance with a maximum at 60 K to a negative one at low temperatures. The positive magneto-resistance at high temperatures indicates that the preferred spin orientation of the charge-carrier holes is different in the ferromagnetic MnAs cluster with respect to the paramagnetic GaAs:Mn matrix. At low temperatures the electrical resistivity in GaAs:Mn layers with MnAs clusters is larger than in GaAs:Mn layers without clusters. This can be explained by the trapping of the charge-carrier holes at the interface between the MnAs clusters and the GaAs:Mn matrix. Application of an external magnetic field lifts the trapping and hence results in a negative magneto-resistance. The hole trapping can also explain the additional broad absorption signal. Each localized hole spin gives rise to paramagnetic resonance. Depending on the position where they are trapped, the hole spins experience a broad distribution of local fields due to crystal anisotropy and magnetization. These local fields add to the external field and give rise to different resonance conditions for each hole. Hence the absorption is broadened at least over the full range of magnetic fields between zero and the anisotropy field. Finally it is important to note that both the observed magneto-resistance behaviour and the additional low-temperature signal are best visible for the thinnest layer and are strongly suppressed with increasing layer thickness, which supports the correlation between both effects.

5. Conclusions

Ferromagnetic resonance was used to study the magnetic properties of MOVPE-grown paramagnetic–ferromagnetic granular hybrid layers (thickness 150 nm $\leqslant d \leqslant$ 1000 nm) consisting of ferromagnetic MnAs clusters embedded in a paramagnetic GaAs:Mn matrix. The angular and the field dependence of the observed ferromagnetic resonance curves of the MnAs clusters can be modelled using the classical equation of motion for the magnetization and accounting for Zeeman, magneto-crystalline anisotropy and demagnetization effects. All MnAs clusters grow with their hexagonal c-axis approximately along the cubic GaAs [111] and the three corresponding directions. The differences of the resonance behaviour observed for the various samples under study can be entirely described by the variation of demagnetization

factors due to different dominant cluster shapes. Assuming a rotational ellipsoidal shape of the clusters allows one to fit the resonance curves by varying the height-to-width ratio of the axes of the ellipsoid. With increasing layer thickness the dominant cluster shape changes from a lens shape to a spherical shape. The latter shape appears to be the final stage of the shape transformation of the clusters for the MOVPE growth conditions used. These results are corroborated by transmission-electron microscope studies on the same samples. The temperature dependence of the magnetic resonance spectra reveals an additional broad absorption signal below 60 K, which can be ascribed to hole spins localized at the interface between MnAs clusters and GaAs:Mn matrix. The analysis demonstrates that the magnetic properties of the mesoscopic hexagonal MnAs clusters can be tuned by controlling the shape of the clusters in the growth process.

Acknowledgments

We are grateful for funding by the Bundesministerium für Bildung und Forschung (BMBF) via the contract numbers VDI/EKM 13N6917 and VDI/Spintronics 13N8281 as well as by the Deutsche Forschungsgemeinschaft (DFG) via Sonderforschungsbereich SFB 484 (Augsburg) and project no KL 1289/4-1. TK was supported by the European graduate college 'Electron–electron interactions in solids'.

References

[1] Prinz G A 2000 *Science* **250** 1092
[2] Ohno H, Matsukura F and Ohno Y 2001 *Solid State Commun.* **119** 281
[3] Tanaka M 2002 *Semicond. Sci. Technol.* **17** 327
[4] Nazmul A M, Sugahara S and Tanaka M 2003 *Phys. Rev.* B **67** 241308
[5] Wang K Y, Campion R P, Edmonds K W, Sawicki M, Dietl T, Foxon C T and Gallagher B L 2005 *AIP Conf. Proc.* **772** 333
[6] Jungwirth T, Wang K Y, Mašek J, Edmonds K W, König J, Sinova J, Goncharuk N A, MacDonald A H, Sawicki M, Rushforth A W, Campion R P, Zhao L X, Foxon C T and Gallagher B L 2005 *Phys. Rev.* B **72** 165204
[7] Lampalzer M, Nau S, Pietzonka C, Treutmann W, Volz K and Stolz W 2004 *J. Cryst. Growth* **272** 772
[8] Couto O D D Jr, Brasil M J S P, Iikawa F, Giles C, Adriano C, Bortoleto J R R, Pudenzi M A A, Gutierrez H R and Danilov I 2005 *Appl. Phys. Lett.* **86** 071906
[9] Moreno M, Trampert A, Jenichen B, Däweritz L and Ploog K H 2002 *J. Appl. Phys.* **92** 4672
[10] Yokoyama M, Yamaguchi H, Ogawa T and Tanaka M 2005 *J. Appl. Phys.* **97** 10D317
[11] Moreno M, Jenichen B, Däweritz L and Ploog K H 2005 *J. Vac. Sci. Technol.* B **23** 1700
[12] De Boeck J, Oesterholt R, Bender H, Van Esch A, Bruynseraede C, Van Hoof C and Borghs G 1996 *J. Magn. Magn. Mater.* **156** 148
[13] Shimizu H, Miyamura M and Tanaka M 2001 *Appl. Phys. Lett.* **78** 1523
[14] Takamura K, Matsukura F, Ohno Y and Ohno H 2001 *J. Appl. Phys.* **89** 7024
[15] Akinaga H, Miyanishi S, Tanaka K, Van Roy W and Onodera K 2000 *Appl. Phys. Lett.* **76** 97
[16] Ando K, Chiba A and Tanoue H 1998 *Appl. Phys. Lett.* **73** 387
[17] Chen C, Cai M, Wang X, Xu S, Zhang M, Ding X and Sun Y 2000 *J. Appl. Phys.* **87** 5636
[18] Wellmann P J, Garcia J M, Feng J-L and Petroff P M 1997 *Appl. Phys. Lett.* **71** 2532
[19] Wellmann P J, Garcia J M, Feng J-L and Petroff P M 1998 *Appl. Phys. Lett.* **73** 3291
[20] Akinaga H, De Boeck J, Borghs G, Miyanishi S, Asamitsu A, Van Roy W, Tomioka Y and Kuo L H 1998 *Appl. Phys. Lett.* **72** 3368
[21] Schmidt D R, Petukhov A G, Foygel M, Ibbetson J P and Allen S J 1999 *Phys. Rev. Lett.* **82** 823
[22] Mizuguchi M, Akinaga H, Ono K and Oshima M 2000 *J. Appl. Phys.* **87** 5639
[23] Park Y D, Wilson A, Hanbicki A T, Mattson J E, Ambrose T, Spanos G and Jonker B T 2001 *Appl. Phys. Lett.* **78** 2739
[24] Miyoshi T, Matsui T, Tsuda H, Mabuchi H and Morii K 1999 *J. Appl. Phys.* **85** 5372

[25] Kang J-S, Kim G, Wi S C, Lee S S, Choi S, Sunglae Cho, Han S W, Kim K H, Song H J, Shin H J, Sekiyama A, Kasai S, Suga S and Min B I 2005 *Phys. Rev. Lett.* **94** 147202
[26] Li A P, Shen J, Thompson J R and Weitering H H 2005 *Appl. Phys. Lett.* **86** 152507
[27] Li A P, Wendelken J F, Shen J, Feldman L C, Thompson J R and Weitering H H 2005 *Phys. Rev.* B **72** 195205
[28] Ye S, Klar P J, Hartmann Th, Heimbrodt W, Lampalzer M, Nau S, Torunski T, Stolz W, Kurz K, Krug von Nidda H-A and Loidl A 2003 *Appl. Phys. Lett.* **83** 3927
[29] Shimizu H and Tanaka M 2002 *Appl. Phys. Lett.* **81** 5246
[30] Shimizu H and Tanaka M 2001 *J. Appl. Phys.* **89** 7281
[31] Hartmann Th, Lampalzer M, Klar P J, Stolz W, Heimbrodt W, Krug von Nidda H-A, Loidl A and Svistov L 2002 *Physica* E **13** 572
[32] Gönnenwein S T B, Graf T, Wassner T, Brandt M S, Stutzmann M, Philipp J B, Gross R, Krieger M, Zürn K, Ziemann P, Köder A, Frank S, Schoch W and Waag A 2003 *Appl. Phys. Lett.* **82** 730
[33] Liu X, Sasaki Y and Furdyna J K 2003 *Phys. Rev.* B **67** 205204
[34] Sasaki Y, Liu X, Furdyna J K, Palczewska M, Szczytko J and Twardowski A 2002 *J. Appl. Phys.* **91** 7484
[35] Lampalzer M, Volz K, Treutmann W, Nau S, Torunski T, Megges K, Lorberth J and Stolz W 2003 *J. Cryst. Growth* **248** 474
[36] Lampalzer M, Volz K, Treutmann W, Nau S, Torunski T, Megges K, Lorberth J and Stolz W 2002 *Inst. Phys. Conf. Ser.* **170** 249
[37] Volz K, Lampalzer M, Schaper A, Zweck J and Stolz W 2001 *Inst. Phys. Conf. Ser.* **169** 211
[38] De Blois R W and Rodbell D S 1963 *J. Appl. Phys.* **34** 1101
[39] Gmelin L 1983 *Gmelin Handbook of Inorganic and Organometallic Chemistry* 8th edn, vol 56, C9 ed H Katscher *et al* (Berlin: Springer) (ISBN 3540934693)
[40] Gurevich A G and Melkov G A 1996 *Magnetization Oscillations and Waves* (Boca Raton, FL: CRC Press) (ISBN 0849394600)